Dynamic Investigation of Multi-Component Force Sensors using Harmonic Excitation

Yon-Kyu Park[*], Rolf Kumme[**] and Dae-Im Kang[*]
[*]Korea Research Institute of Standards and Science(KRISS), P.O.BOX 102, Yusong, Taejon 305-600, Korea
[**]Physikalisch-Technische Bundesanstalt(PTB), Bundesallee 100, 38116 Braunschweig, Germany

Abstract

This paper describes the dynamic investigation of a 3-component and a 6-component force-moment sensors using the facilities in the PTB (Physikalisch-Technische Bundesanstalt) in Germany. The 3-component sensor has the transverse forces F_x and F_y of each having 200 N capacity and a twisting moment M_z of 10 Nm capacity and the 6-component sensor has force components F_x, F_y and F_y each having 200 N capacity and moment components M_x, M_y and M_z each having 20 Nm capacity. The sensitivity of the sensors decreases as the frequency increases and the sensors show almost 90^o symmetry due to their geometry.

1. Introduction

The physical quantity force is a vector that has a magnitude as well as a direction. A mechanical load can be divided into six components: 3 force components and 3 moment components. Therefore, in order to define a force quantity completely, it is necessary to know the value of all of its six components. A multi-component force-moment sensor is a device that enables forces and moments to be measured simultaneously.

A multi-component force-moment sensor should be accurately evaluated before it is practically employed in the robot, machine tool and automobile fields. The static evaluation of the multi-component sensor can be done by using a multi-component force calibration machine. However, because the multi-component sensor is often used in dynamic mode, its dynamic evaluation is very important.

There are two kinds of methods to investigate the dynamic characteristics of a force sensor. One is a harmonic excitation method[1-4] and the other is an impact excitation method[5-7]. Among the two methods, we used the harmonic excitation method by using a shaker system and a multi-channel dynamic analyser system in this paper. The dynamic investigation of a 6-component force-moment sensor subjected to impulse force will be presented in [8].

This paper describes the dynamic investigation of a 3-component[9-11] and a 6-component[12, 13] force-moment sensors using the facilities in the PTB in Germany.

2. Multi-component force-moment sensors

Figure 1 shows the schematic diagram of the 3-component force-moment sensor. The capacity of the sensor is 200 N for the transverse force components F_x and F_y respectively, and 10 Nm for the component of twisting moment M_z. Strain gauges XC1 and XC2 detect the compression strain for the transverse force F_x and strain gauges XT1 and XT2 detect the tensile strain for the transverse force F_x. Strain gauges YC1, YC2, YT1 and YT2 measure the transverse force F_y and strain gauges ZC1, ZC2, ZT1 and ZT2 measure the twisting moment M_z. The sensing element was made of Al 2024-T4. And it was manufactured by using

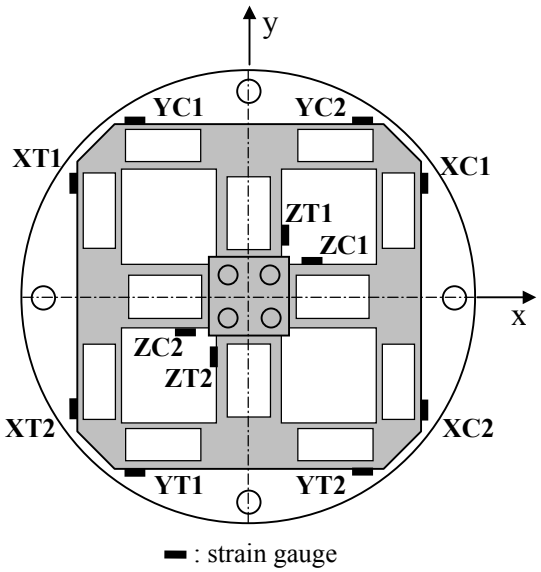

Figure 1. Schematic diagram of a 3-componentforce-moment sensor.

the process of electric discharge machining and wire cutting machining.

The sensitivity of the sensor is 2.5158×10^{-3} (mV/V)/N for F_x, 2.5380×10^{-3} (mV/V)/N for F_y and 5.1404×10^{-3} (mV/V)/(Nm) for M_z. The largest static interference error is about 0.99 %.

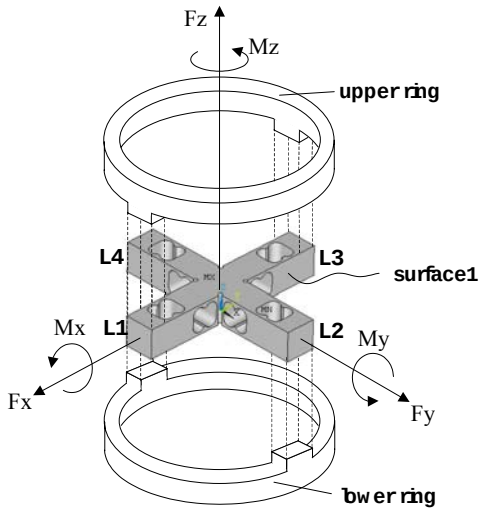

Figure 2. Configuration of the binocular type 6-component force-moment sensor

Figure 2 shows the configuration of the binocular type 6-component force-moment sensor. The sensing unit has upper and lower rings, which each have numerous diametrically opposite connectors and locking holes. The sensing unit also has a cross beam which has horizontal and vertical parts crossing at right angles. In the cross beam, numerous vertical and transverse binocular openings are formed on the horizontal and vertical parts and each have a binocular cross-section. The horizontal and vertical parts of the cross beam are spaced apart from the lower and upper rings by a gap, but are connected to the upper and lower rings through the connectors, thus integrating the sensing unit into a single structure. The ends of the horizontal part of the cross beam are attached to the upper ring and the ends of the vertical part are attached to the lower ring. This results in a difference in the boundary conditions of the horizontal and vertical parts. Therefore, the 6-component force-moment sensor has an asymmetry in the horizontal and vertical directions although the sensing element of the cross beam has a 90° symmetrical geometry.

The sensitivity of the sensor is 2.6084×10^{-3} (mV/V)/N for F_x, 2.5905×10^{-3} (mV/V)/N for F_y, 2.3597×10^{-3} (mV/V)/N for F_z, 4.3040×10^{-3} (mV/V)/(Nm) for M_x, 4.3217×10^{-3} (mV/V)/(Nm) for M_y and 2.9265×10^{-3} (mV/V)/(Nm) for M_z. Coupling errors between all components are less than 3%.

3. PTB facilities for dynamic force

When force transducers are used for dynamic measurements, errors of several percent and more can occur because of the unknown dynamic response of the force transducer. Therefore the dynamic sensitivity of a force measuring device:

$$S = \frac{U_v}{F} \qquad (1)$$

must be determined from the ratio of the output signal of the force measuring device U_v and the acting dynamic force F, which must be well known. Because force standard machines are designed for static force measurement they can not be used for dynamic investigations. Special facilities and measurement procedures were therefore developed at PTB to investigate the dynamic behaviour of force measuring devices [1, 2]. The principle of the dynamic calibration of force measuring devices is based on a defined realisation of mass forces. So the force transducer to be calibrated is mounted on an electrodynamic shaker, and a load mass is screwed onto the force transducer as shown in figure 3.

Excitation by the shaker results in a dynamic force F acting on the force transducer:

$$F = (m_l + m_e)\cdot \ddot{x}_1 \qquad (2)$$

where $\ddot{x}_1$ is the acceleration of the load mass m_l and the end mass m_e of the force transducer . The simple Eq. (2) does not take the effects of the relative motions of the load mass into account, or the influence of side force which must be considered because force is a vector quantity. Side forces can be reduced by using air bearings. To allow for the influence of relative motion, the dynamic force must be determined from the acceleration distribution $a(x,t)$ and the mass distribution of density ρ according to

$$F = \int_V \rho \cdot a(x,t)\cdot dV \quad . \qquad (3)$$

For the determination of the acceleration distribution, multi-component acceleration measurements are necessary as shown in Figure 3, and the theory presented in [2,3] must be used to calculate the dynamic force. According to Eq. (2) or, more accurately, according to Eq. (3), the dynamic force is traceable to the definition of the force according to Newton's law. The dynamic sensitivity of the whole force measuring device includes the frequency response of force transducer and measuring amplifier [4].

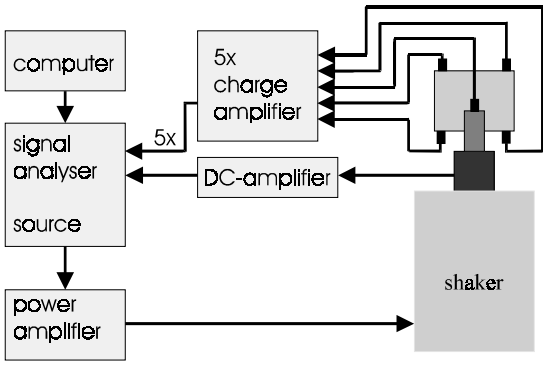

Figure 3. Calibration principle for dynamic force measurement.

4. Experiment

Figure 4 shows the schematic diagram of the experimental setup to analyse the dynamic characteristics of the normal force component F_z of the 6-component force-moment sensor. The sensor is mounted looking upwards on a shaker system (B&K 4802 + B&K 4818) so that the normal force direction of the sensor coincides with the vertical direction of the shaker. An external mass of 0.9 kg is attached to the top of the force-moment sensor. A disk type adapter is used for the 6-component force-moment sensor. The external mass has the role of activating dynamic force by oscillating the shaker vertically. The external mass is made of steel. Two accelerometers (a_{m1} and a_{m2}, B&K 8305) are mounted on top of the attached mass to measure the acceleration of the mass. An accelerometer(a_b, Kistler 8002K) is used to measure the acceleration signal of the base as shown in Figure 4.

The three acceleration signals are passed to charge amplifiers (B&K 2626). Three force/ moment signals, always including the F_z component from the 6-component force-moment sensor, are passed to a dynamic amplifier HBM MGC with DC amplifier MC10. Then, all the acceleration and force/moment signals are connected to a multichannel FFT analyser system HP 3565A. The analyser controls the shaker system through a power amplifier B&K 2708.

Figure 5 shows the schematic diagram for analysis of the dynamic characteristics of the

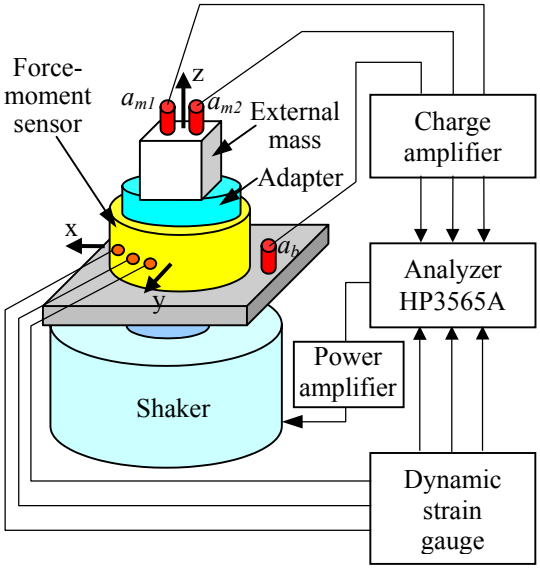

Figure 4. Schematic diagram of the experimental setup for the normal force component F_z.

transverse force components F_x and F_y. Force-moment sensors are mounted on the shaker using a vertical adaptor to make the transverse force direction of the sensor coincide with the vertical direction of the shaker. An external mass is attached to the sensor and an accelerometer (a_m, B&K 8305) is mounted on the mass. Two accelerometers (a_b and a_a, Kistler 8002K) are used to measure the acceleration signals of the base (a_b) and the top of the adapter (a_a) as shown in figure 5. A counter mass is assembled on the adaptor to reduce the rolling motion.

Figures 6 and 7 show the experimental setup to investigate moment components of the force-moment sensors. Figure 6 is for M_x and M_y and figure 7 is for M_z. A beam of length 0.1 m is used to activate dynamic moment. The beam is made of aluminium and its cross-sectional dimension is 18×18 mm. One end of the beam

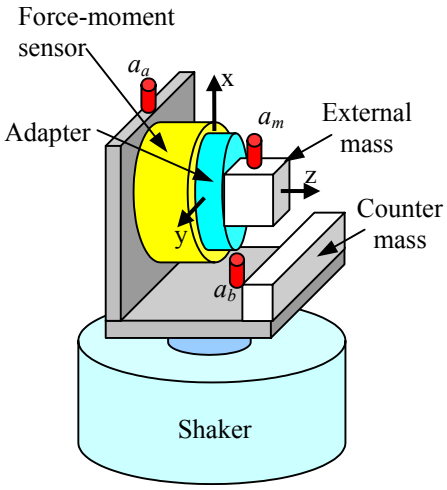

Figure 5. Experimental setup to examine the transverse force components F_x and F_y.

is attached to the centre of the sensor and an external mass is mounted at the other end of the beam. An accelerometer is mounted at the front of the beam (a_c, Kistler 8002K) and another is mounted on the external mass (a_m, B&K 8305).

The frequency response functions(FRF) are measured by using the sine sweep method. A sine sweep is a method to activate sine signal with increasing frequency of a specified rate and measure the responses at the activating frequency. The measurements are performed at every 10 Hz from 20 Hz to 1000 Hz. At each measuring frequency, an average of 20 cycles were performed.

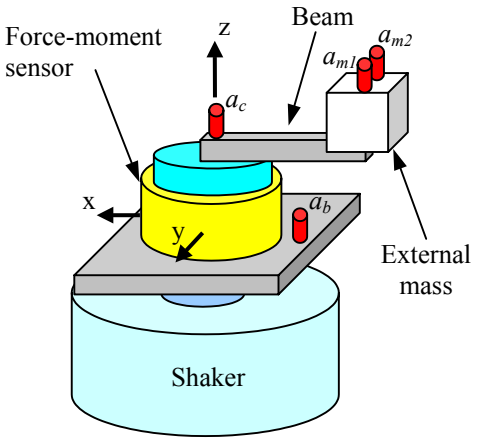

Figure 6. Experimental setup to examine the moment components M_x and M_y.

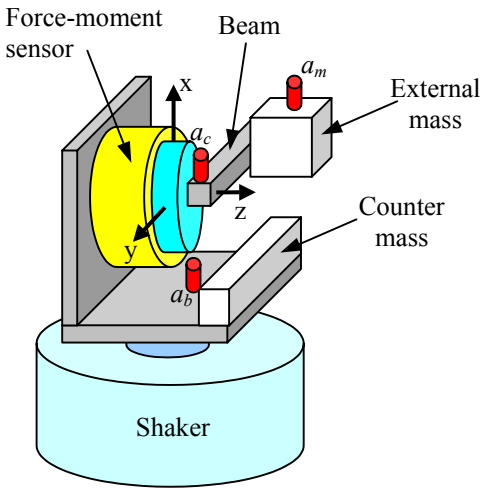

Figure 7. Experimental setup to examine the moment component M_z.

5. Measurement results of a 3-component force-moment sensor

5.1 Preliminary investigation

The sensitivity of a force-moment sensor is defined as the ratio of the electrical output to the real applied force or moment. The sensitivity can be estimated as a function of frequency. The actual applied force can be estimated as the product of the acceleration and the equivalent mass according to Newton's second law. The acceleration can be measured by the accelerometer mounted on the external mass. The equivalent mass is the sum of the external mass, the mass of the accelerometer, the mass of the screws to assemble the external mass and the internal mass of the 3-component force-moment sensor.

The real moment can be estimated as follows:

$$M_{\mathrm{a}} = m_{\mathrm{ext,equ}} \cdot a_{\mathrm{m}} \cdot l + m_{\mathrm{beam}} \cdot \frac{a_{\mathrm{m}} + a_{\mathrm{c}}}{2} \cdot \frac{l}{2} + I_{\mathrm{iz}} \cdot \frac{a_{\mathrm{m}} - a_{\mathrm{c}}}{l} \quad (4)$$

where M_a is the real moment and $m_{ext,equ}$ is the equivalent external mass, i.e. the sum of the external mass, the mass of the accelerometer mounted on the external mass and the mass of the screws for assembly. m_{beam} is the mass of the beam, I_{iz} is the internal moment of inertia for the M_z component, a_m is the acceleration at the external mass, a_c is the acceleration at the front end of the beam and l is the length of the beam.

The internal mass of the sensor was measured statically. To measure the internal mass along

the x-direction, we mounted the sensor with the x-axis of the sensor upwards. We measured the F_x signal without the external mass. Then we inverted the sensor by 180° and measured the F_x signal again. The internal mass for the F_x component can then be estimated as follows:

$$m_{\mathrm{ix}} = \frac{\left|F_{\mathrm{x}+} - F_{\mathrm{x}-}\right|}{2g_{\mathrm{loc}}} \qquad (5)$$

where m_{ix} is the internal mass for the F_x component, g_{loc} is the local acceleration of gravity and F_{x+}, F_{x-} are the force values of the two measurements. The internal mass for the transverse force F_y component can be measured in similar fashion. The measured internal masses are 97.6 g and 83.8 g for the F_x and F_y components respectively.

The internal moment of inertia was estimated using a similar method. But in this case we attached a beam and an external mass to the sensor to activate the component of twisting moment M_z. The internal moment of inertia was estimated as follows:

$$I_{\mathrm{iz}} = \frac{\left|M_{\mathrm{z}+} - M_{\mathrm{z}-}\right|}{2g_{\mathrm{loc}}} \qquad (6)$$

where M_{z+}, M_{z-} are the moment values of the two measurements. The measured internal moment of inertia is 98.6 g•m.

5.2 Investigation of transverse forces

The investigation of transverse force components was carried out using the experimental setup illustrated in figure 5.

Figure 8 shows the FRFs of the force and moment signals (F_x, F_y, M_z) and the acceleration signal of the external mass(a_m) with respect to the base acceleration signal(a_b) for the examination of the transverse force component F_x. In all FRFs one can find a large peak at 250 Hz which is the first resonant frequency. In the FRFs of the force signals and acceleration signal there is another peak at 580 Hz. However, this peak does not appear in the FRF of the moment signal M_z. In the FRF of the moment signal there is a peak at 650 Hz that cannot be seen in other FRFs. This frequency may be a related twisting mode, which therefore does not appear in other FRFs.

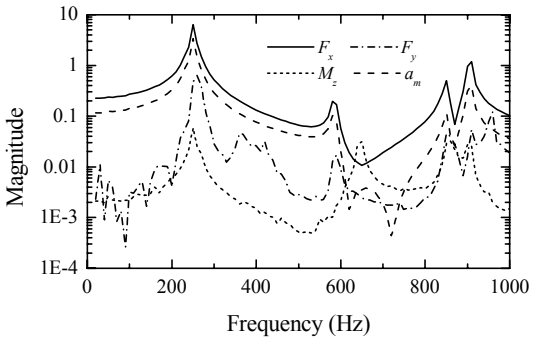

Figure 8. Frequency response functions during examination of the transverse force component F_x.

Figure 9(a) is the dynamic sensitivity of the transverse force component F_x normalized to its static sensitivity. The sensitivity comes close to 1 at low frequency and decreases with frequency until about 550 Hz, i.e. the operational frequency range of the sensor. In contrast, above that frequency the sensitivity increases and shows complicated features. In addition to this, there are several peaks in the sensitivity. These peak frequencies coincide with the anti-resonant frequency of the acceleration. The sensitivity is the ratio of the electrical output of the sensor to the real force which is the product of the equivalent mass and the acceleration. Therefore, at the anti-resonant frequency of the acceleration there are peaks in the sensitivity.

Figure 9(b) shows the interference between F_x and F_y and interference between F_x and M_z. The interference is defined as the ratio of the electrical output of the comparative component (F_y or M_z) to that of the F_x component. Within the operational frequency range of the sensor, the interferences are much less than 1. Of the two, the interference between F_x and M_z shows the lower value.

We performed the dynamic measurement for the investigation of the transverse force component F_x by inverting the sensor by 180°. The measured results are quite similar to figure 9. When we examine the transverse force component F_y, we obtain similar results to figure 9.

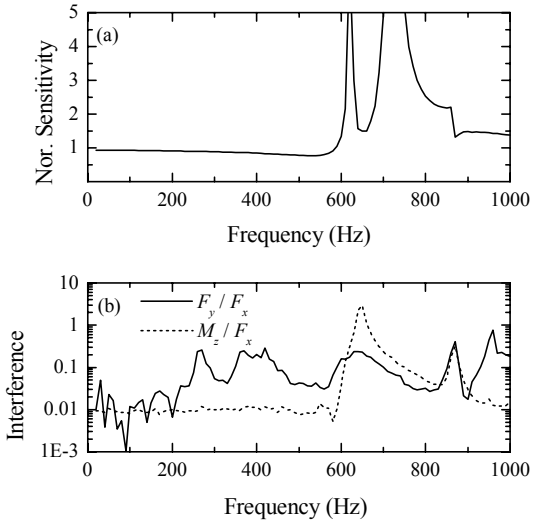

Figure 9. Sensitivity and interference of the transverse force component F_x; (a) sensitivity; (b) interference.

5.3 Investigation of the twisting moment

The investigation of the component of twisting moment was carried out using the experimental setup illustrated in figure 7.

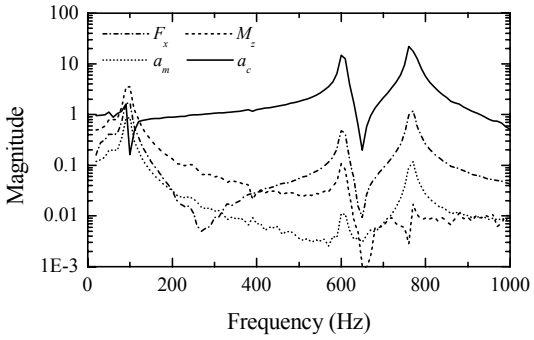

Figure 10. Frequency response functions forthe component of twisting moment M_z.

Figure 10 shows FRFs of the force and moment signals (F_x, M_z), and the acceleration signals at the external mass (a_m) and at the front of the beam(a_c) with respect to the base acceleration signal(a_b) for the examination of the component of twisting moment M_z. Here, the sensor is mounted with the +x axis of the sensor pointing downwards. The beam is mounted in the direction of the –y axis of the sensor. From the FRFs one can see that there are 3 peaks the frequencies of which are 100 Hz, 600 Hz and 770 Hz. Among them, the peak at 100 Hz has a high value at the FRF of the acceleration at the external mass, but it does not appear at the FRF of the acceleration at the front of the beam. This means that the relative motion of the external mass and the beam dominates the motion of the sensor at that frequency. At higher frequency, the motion of the sensor itself becomes larger.

Figure 11(a) is the dynamic sensitivity of the component of twisting moment M_z, normalized to its static sensitivity. The sensitivity seems to tend towards 1 at low frequencies and decreases rapidly as the frequency increases. Figure 11(b) shows the interference between M_z and F_x and the interference between M_z and F_y. The interferences are less than 1 in the low frequency range. Because the sensor, the beam and the external mass oscillate along the x-axis of the sensor, there is an undesired transverse force component F_x. Therefore, in the estimation of the interference between M_z and F_x, the F_x component is compensated.

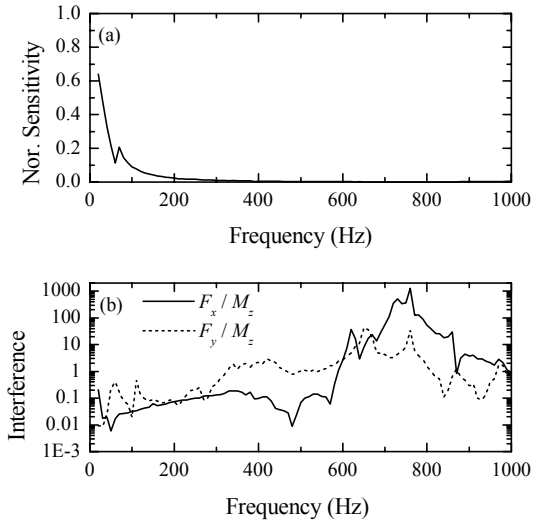

Figure 11. Sensitivity and interference of the component of twisting moment M_z; (a) sensitivity; (b) interference.

When we change the direction of the beam by 180°, we can get similar results. And even when we change the direction of the sensor by 90° to turn the +y axis of the sensor downwards, we get similar results.

6. Measurement results of a 6-component force-moment sensor

6.1 Preliminary investigation

The internal mass and internal moment of inertia can be estimated as like 5.1. The measured internal masses are 539.7 g, 522.4 g and 546.5 g for the F_x, F_y and F_z components respectively. The measured internal moment of inertia are 149.8 g·m, 80.1 g·m and 97.3 g·m for the M_x, M_y and M_z components respectively.

6.2 Investigation of the force component F_z

The normal force component was determined by using the experimental setup illustrated in figure 4.

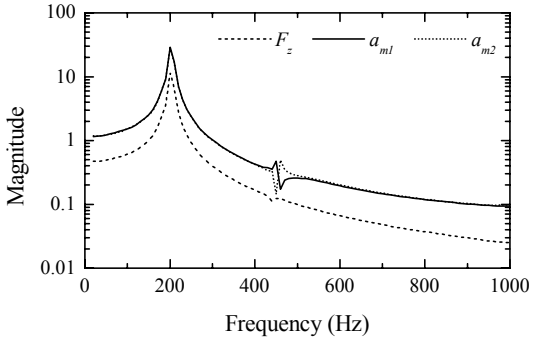

Figure 12. Frequency response functions when examining the normal force component F_z.

Figure 12 shows FRF's of the force signal F_z and the acceleration signals at the external mass (a_{m1}, a_{m2}) with respect to the base acceleration signal (a_b). In the figure the FRFs are not scaled to represent physical quantities but are estimated from the electrical signals. This is the same for all other FRFs in this paper. For all FRFs there is a sharp peak at 200 Hz, which is a resonance. In the FRFs of the acceleration signals there is some kind of disturbance at about 450 Hz. At that frequency the two accelerations show opposite behaviour, so that one increases as the other decreases. The two accelerometers are mounted along the y-axis, therefore one can see that there is a rocking motion along the y-axis.

Figure 13(a) is the dynamic sensitivity of the normal force component F_z normalized to its static sensitivity. We take the mean of the two accelerations to estimate the sensitivity. The sensitivity is close to 1 at low frequency, then decreases with frequency slowly until about 420 Hz, when the rocking motion occurs. After that frequency value the sensitivity shows a disturbance and decreases fast with frequency. The operational frequency range for the F_z component is restricted to about 420 Hz.

Figure 13(b) shows the interferences between F_z and other force/moment components. The interference is defined as the ratio of electrical output of comparative components to the electrical output of the F_z component. Within the operational frequency range 420 Hz, the interference is less than 1. When the rocking motion occurs at about 450 Hz, the interference shows a higher value than 1.

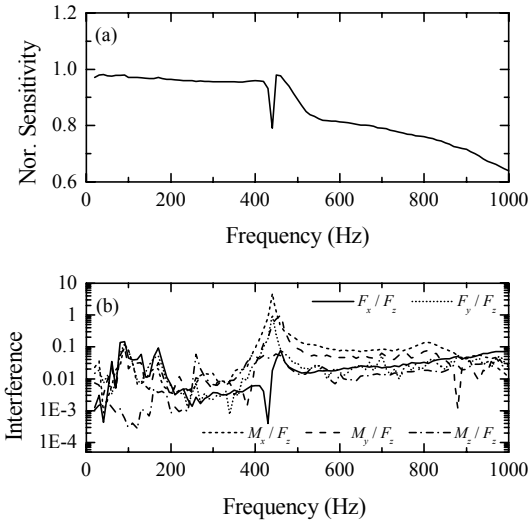

Figure 13. Sensitivity and interference of the normal force component F_z; (a) sensitivity; (b) interference.

6.3 Investigation of force components F_x and F_y

The determination of the transverse force components F_x and F_y was done by using the experimental setup illustrated in figure 5.

Figure 14(a) shows FRFs of the force and moment signals (F_x, M_y) and the acceleration signal of the external mass (a_m) with respect to the base acceleration signal (a_b) for the the transverse force component F_x. In the FRFs one can find high peaks at 110 Hz and 400 Hz. Figure 14(b) shows the FRFs for the examination of the transverse force component F_y. There are two peaks at 110 Hz and 410 Hz. The tendency is similar to figure 14(a). However, there are two remarkable differences:

the second peak frequency at 410 Hz is different from figure 14(a) and, in the FRF of the moment component M_x, the peak at 410 Hz has a very low value.

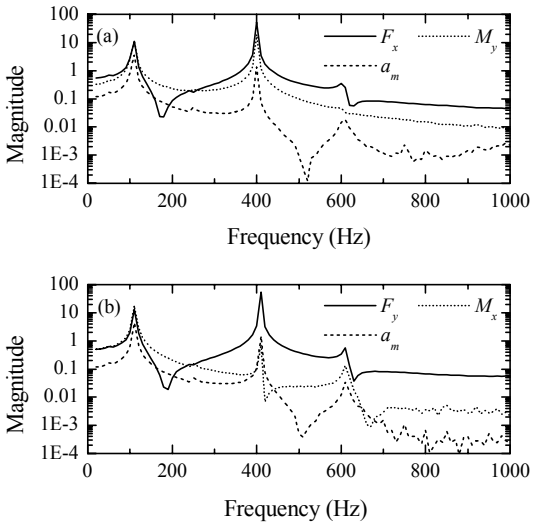

Figure 14. Frequency response functions when examining the transverse force components F_x and F_y.; (a) for F_x; (b) for F_y.

The geometrical asymmetry of the force-moment sensor causes the discrepancy between figures 14(a) and (b) as mentioned before. As one can easily see in figure 2, ends of the x-directional part of the cross beam are attached to the upper ring. Ends of the y-directional part are attached to the lower ring. The boundary conditions of the x- and y-directional parts of the cross beam are different. The F_x and M_x components are transferred to the y-directional part through the centre while both its ends are fixed. In contrast, the the F_y and M_y components are transferred to the x-directional part through both ends while its centre is fixed. The geometrical asymmetry due to the different boundary conditions causes different dynamic behaviours.

For the FRFs of the moment signals, the first peak has a higher value than the second peak. In contrast, for the FRFs of the force signals the second peak has a higher value than the first. Therefore, one may note that the first peak arises mainly from the rotating motion and the second mainly from the transverse motion.

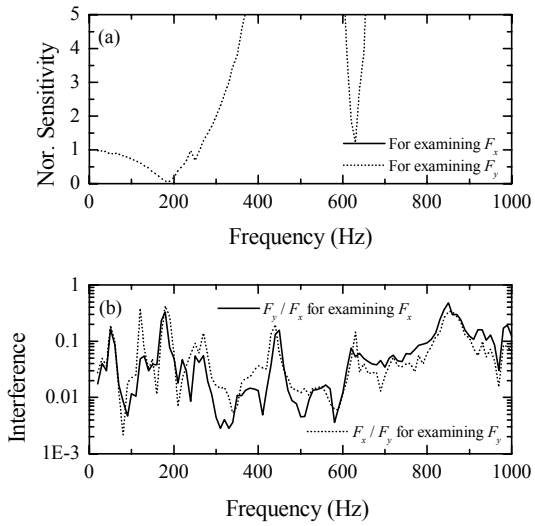

Figure 15. Sensitivities and interference of the transverse force components F_x and F_y; (a) sensitivity; (b) interference.

Figure 15(a) shows the dynamic sensitivities of the transverse force components F_x and F_y normalized to their static sensitivities. The sensitivities are similar. The sensitivity comes close to 1 at low frequency and decreases with the frequency until about 170 Hz. Above that frequency, on the other hand, the sensitivity increases and shows complex features. In addition to that, there is a sharp peak in the sensitivity at 520 Hz although it is not represented in the figure. This peak frequency coincides with the anti-resonant frequency of the acceleration. The sensitivity is the ratio of the electrical output of the sensor to the actual force that is the product of equivalent mass and the acceleration. Therefore, at the anti-resonant frequency of the acceleration, there are peaks in the sensitivity. The operational frequency range of the force components F_x and F_y is restricted to about 100 Hz at which the sensitivity decreases to about 70% of its static sensitivity. The sensitivity of 70% implies half power.

Figure 15(b) shows the interference between F_x and F_y,i.e. the ratio of electrical output of F_y to that of F_x in the examination of the F_x component, and the reverse for the F_y component. The interference is less than 1.

We performed a dynamic measurement for the determination of the transverse force

components $-F_x$ and $-F_y$ by inverting the sensor by 180°. The measured results are quite similar to those shown in figure 15.

6.4 Investigation of the moment components

The investigation of the moment components M_x and M_y was carried out using the experimental setup illustrated in figure 6. The investigation of the moment components M_z was carried out using the experimental setup illustrated in figure 7.

For all the moment components, the sensitivity seems to tend towards 1 at low frequency and decreases rapidly as the frequency increases. The operational frequency range is restricted to a narrow band.

7. Conclusions

We investigated the dynamic characteristics of a 3-component and a 6-component force-moment sensors. To do so, we used a harmonic excitation system consisting of a shaker system and a multi-channel dynamic analyser.

The dynamic sensitivity decreases with the frequency. In particular, for the moment components the sensitivity decreases rapidly, therefore the sensor has poor ability to measure dynamic moment. There may be many reasons for this phenomenon. Among them, the interference caused by the mechanical structure of the sensor is a significant candidate. Because of the interference, some part of the input energy should be converted to other types of motion. As the interference increases with the frequency, the sensitivity decreases with the frequency.

The 3-component force-moment sensor shows 90° symmetrical dynamic characteristics because of its symmetric geometry. The 6-component force-moment sensor not only shows 90° symmetrical dynamic characteristics, but also asymmetrical properties in the x- and y-axes because of its geometry.

The FRFs in this paper represent the dynamic characteristics of the 6-component force-moment sensor. However, detailed interpretation of the FRFs is omitted in this paper because the main theme of this paper is focused on the dynamic sensitivity of the sensor.

The uncertainty of this dynamic measurement is very important, because the confidence of a measurement can be guaranteed by its uncertainty. However, the main aim of this paper is to show first results that demonstrate how complicated and complex the dynamic properties of a multi-component force-moment sensor is. The aim of this paper is to introduce dynamic phenomena of a multi-component force sensor and the measurement uncertainty will be analysed in another paper.

The force-moment sensor was designed and developed from static considerations only. The stiffness of the sensor is very low, hence its frequency range is restricted to a narrow band. Therefore, it is desirable to develop a multi-component force-moment sensor with an extended frequency range that is suitable for various dynamic applications.

ACKNOWLEDGEMENTS

This work has been supported by the National Research Laboratory for the Force Measurement & Evaluation (Project No. 2000-N-NL-01-C-141).

References

[1] Kumme R., Peters M. and Sawla A. 1995 Improvements of dynamic force calibration *Part 2. Brussels, Luxembourg: Commission of the European Communities(BCR information, Report EUR No. 16497EN) ISBN 92-827-5344-1* 122.

[2] Kumme R. 1996 Untersuchungen eines direkten Verfahrens zur dynamischen Kalibrierung von Kraftmeßgeräten - ein Beitrag zur Verringerung der Meßunsicherheit *Dissertation, Technische Universität Braunschweig (PTB-Bericht MA-48) ISBN 3-89429-744-1* 170.

[3] Kumme R. Oktober 7-11 1996 The determination of the effective dynamic force for the calibration of force transducers, with due regard to the distribution of mass and acceleration *Proceedings of the 15th IMEKO TC3 Conference, Madrid (Spain)* 129-138.

[4] Kumme R. June 2-6 1997 The main influences on the dynamic properties of

force measuring devices *Proceedings of the 14th IMEKO World Congress, Tampere (Finland)* **3** 102-107.
[5] Fujii Y. and Fujimoto H. 1999 Design Note: Proposal for an impulse response evaluation method for force transducers *Meas. Sci. Technol.* **10** N31-N33.
[6] Fujii Y., Fujimoto H. and Namioka S. 1999 Mass measurement under weightless conditions *Review of Scientific Instruments* **70(1)** 111-113.
[7] Fujii Y. and Fujimoto H. 1999 Measurement of frictional characteristics of a pneumatic linear bearing *Meas. Sci. Technol.* **10** 362-366.
[8] Kobusch M., Bruns T., Kumme R. and Park Y.-K. 2002 Preliminary investigations of dynamic responses of a multi-component force-moment sensor subject to ompulse forces *IMEKO TC3, Germany*, to be published.
[9] Park Y.-K., Kumme R. and Kang D.-I. Dynamic investigation of a 3-component force-moment sensor *accepted for publication to Meas. Sci. Technol*.
[10] Kang D.-I., Kim G.-S., Song H.-G. and Lee J.-T. 1997 Characteristic evaluation of 3-component force sensor *Proceedings of IMEKO TC3* 1-6.
[11] Kim G.-S., Kang D.-I., Joung S.-Y. and Joo J.-W. 1997 Design of sensing element for 3-component load cell using parallel plate structure *J. Korean Soc. Mech. Engng* **15**(9) 127-34.
[12] Kang D.-I., , Jeoung S.-Y. and Joo J.-W. 1987 Design and evaluation of binocular type six-component load cell by using experimental technique *J. of KSME* **21(11)** 1921-1930.
[13] Kim G.-S. 2000 The development of a six-component force/moment sensor testing machine and its evaluation of uncertainty *Meas. Sci. Technol.* **11** 1377-1382.

Contact Person for Paper

Dr. Yon-Kyu Park
Korea Research Institute of Standards and Science, Department of Physical Metrology
P.O.BOX 102, Yusong, Taejon 305-600, Korea
Tel: +82-42-868-5240
Fax: +82-42-868-5249
e-mail: ykpark@kriss.re.kr